This is a repository copy of *Analysis of virtual inerter-based passive absorber for active chatter control*.

White Rose Research Online URL for this paper:
https://eprints.whiterose.ac.uk/221776/

Version: Published Version

Analysis of virtual inerter-based passive absorber for active chatter control

Hakan Dogan [a,b,*], Muhammet Ozsoy [c,d], Erdem Ozturk [e], David J. Wagg [c], Neil D. Sims [c]

[a] Department of Mechanical Engineering, University of Bath, BA2 7AY, Bath, UK
[b] Department of Mechanical Engineering, Hacettepe University, 06800, Ankara, Turkey
[c] Department of Mechanical Engineering, The University of Sheffield, S1 3JD, Sheffield, UK
[d] Department of Mechanical Engineering, Eskisehir Technical University, 26555, Eskisehir, Turkey
[e] Advanced Manufacturing Research Center, The University of Sheffield, Wallis Way, Rotherham, S60 5TZ, Sheffield, UK

ARTICLE INFO

ABSTRACT

This paper presents a novel approach to active chatter control in milling operations using a new concept called the virtual inerter-based dynamic vibration absorber (VIDVA). While passive control methods, such as tuned mass damper (TMDs), have their merits, they may not provide optimal performance and adaptability in certain scenarios. Moreover, the realisation of an idealised inerter-based absorber as a localisation addition can be a difficult task to achieve. In response of these challenges, the integration of the inerter concept into virtual passive absorber (VPA) control to improve chatter stability performance is proposed. Four IDVAs are numerically evaluated to enhance the absolute chatter stability limit, and the numerical results are experimentally validated using cutting tests with a proof-mass actuator providing the control force. The study also includes robustness and actuator saturation analysis to provide a comprehensive evaluation of the proposed virtual IDVA. The findings demonstrate that the virtual IDVA offers improved chatter suppression performance, making it a promising solution for active chatter control and application of IDVAs in milling operations.

1. Introduction

Regenerative chatter is a significant issue in machining operations that hinders productivity by causing excessive vibrations, noise, and poor surface quality. The understanding of the mechanism underlying the regenerative chatter starting in the 1950s [1,2] has led to several methods for chatter suppression. Among them, both passive and active control methods have attracted significant attention.

Earlier attempts for chatter suppression mostly focused on passive methods. For example, Hahn [3] applied a Lanchester damper consisting of a damper with an auxiliary mass. Tobias [4] proposed vibration absorbers for chatter suppression in machine tools. Rivin and Kang [5] introduced a design study for tooling structures, improving the applicability of dynamic vibration absorbers. Tarng et al. [6] utilised a piezoelectric inertia actuator that acts as a tuned mass damper (TMD) in turning such that chatter stability was improved by setting the natural frequency of the device to the natural frequency of the cutting tool. Tlusty [2] revealed that the chatter stability is defined by the real part of the frequency response function (FRF). Following this principle, Sims [7] introduced

analytical solutions that equal the peaks in the real part response, which provides optimal chatter suppression. Later, Miguelez et al. and Rubio et al. [8,9] showed that Sims' method is an effective method for chatter suppression in boring bars. There have been many subsequent research efforts related to TMDs, for example investigating multiple TMDs [10,11], two degree-of-freedom TMDs [12,13], and nonlinear TMDs [14,15] in machining operations.

Recent studies have shown that the inerter-based passive devices demonstrate superior performance compared to TMDs. Smith [16] introduced the inerter in 2002 as a mechanical device that produces a force proportional to the relative acceleration between its terminals. Since then, it has been employed in vehicle suspension systems [17], aircraft landing gears [18,19], and civil engineering applications [20–23]. For machining applications, Wang et al. [24] showed that an inerter-based system can effectively mitigate forced vibration in a milling system. However, the inerter required a grounded connection and was clamped to the work table, which may not be applicable for practical fixturing systems. Most commonly-studied inerter networks (tuned inerter dampers [21], tuned mass damper inerters [22], and tuned viscous mass dampers [20]) in the literature generally require a grounded connection, which limits the versatility of their application into machining. Hu and Chen [25] introduced a set of inerter-based dynamic vibration absorbers (IDVAs) without need for a grounded connection, similar to a classical TMD. Recently, Dogan et al. [26] implemented an IDVA to suppress chatter in a milling operation. The experimental result verified improvement in the absolute stability limit. However, the IDVA design employed in the experiment was not the ideal IDVA proposed in Ref. [25] due to parasitic mass effects and extra stiffness introduced by the mechanical design [27].

Passive control methods, including TMDs, have several merits such as ease of implementation, elimination of need for additional electronic components and complex control systems, and guaranteed stability compared to active control methods. However, these passive methods have limitations in their performance and lack adaptability. To address this drawback, active control methods have been considered in the machine dynamics literature, as well as in the broader structure dynamics community [28]. Researchers have applied active chatter suppression methods to various machine tool components, such as the toolholder-spindle system [29–31], the workpiece [32], the workpiece fixturing system [33], structure of the machine tool [34], and also to robotic-assisted machining [35–37]. Several control methods including direct velocity feedback (DVF) [38,39], linear quadratic regulator [35,40], H_∞ optimisation [41,42], PID [43,44] and μ- synethesis [45,46] have been considered. A comprehensive review including active chatter suppression methods is available in the work of Munoa et al. [47]. To avoid instability, active control methods that reflects passive systems' behaviour, known as 'virtual' passive systems, have been proposed [48]. Huyanan and Sims [49] utilised virtual skyhook control (also known as DVF), virtual passive absorber (VPA) control and virtual passive-active absorber controls to evaluate their chatter suppression performances. They concluded that virtual passive absorbers, which reflect the behaviour of TMDs, outperformed the other two methods. Franco et al. [50] used a virtual passive absorber approach, named virtual passive absorber, to suppression forced vibration in grinding operation. They developed a model-free control law that can be applicable in real-time but the focus was only the forced vibration, not chatter stability.

Integrating the inerter concept into VPA control could potentially improve chatter stability performance. This approach would also enable the detailed examination of idealised IDVA layouts presented in Ref. [25] for chatter suppression without the drawbacks of parasitic mass and extra stiffness introduced by components as well as the physical realisation of the inerter due to small inertance values. Therefore, this paper proposes a new virtual IDVA for active chatter control. A comprehensive analysis of IDVAs using a virtual passive absorber approach to suppress chatter in milling operations is presented. Four IDVAs, which demonstrate vibration suppression improvements compared to a classical TMD (as described in Ref. [25]), are numerically evaluated to enhance absolute chatter stability limit. The numerical results are experimentally validated with cutting tests, where the control force is provided by a proof-mass actuator. Further analyses are conducted for robustness and actuator saturation, presenting a complete analysis.

The rest of the paper is organised as follows. Section 2 introduces the theory of regenerative chatter and IDVAs. Numerical performance evaluation for four IDVA layouts for different mass ratios and experimental validation to justify the analyses in the following sections are presented in Section 3. Section 4 examines the robustness of TMD and IDVAs. Actuator saturation is investigated in Section 5. The results are discussed in Section 6, and finally, a conclusion is drawn.

2. Theory

2.1. Regenerative chatter

The regenerative chatter mechanism is explained using a two degree-of-freedom workpiece and rigid cutting tool as shown in Fig. 1. The cutting tool-workpiece system causes the instantaneous chip thickness, $h(t)$, which varies based on the workpiece's displacements in the previous and current cuts. Assuming the cutting force acting on the tool-workpiece is proportional to the chip area, variations in instantaneous chip thickness result in a dynamic cutting force. The chosen cutting conditions (e.g. depth of cut and spindle speed) could cause instability, leading to exponentially growing cutting forces and associated vibrations.

In orthogonal cutting, the cutting tool is perpendicular to the direction of tool motion, and the cutting forces are often assumed to be proportional to the chip area and a specific cutting coefficient. The tangential and normal cutting forces arise on the cutting edge as shown in Fig. 1 and are defined here as

$$F_t(t) = K_t ah(t), \qquad\qquad F_n(t) = K_n ah(t) \qquad\qquad (1)$$

where K_t, K_n, a and h are the tangential cutting coefficient, the normal cutting coefficient, the axial depth of cut and the chip thickness, respectively. In milling operations, the instantaneous chip thickness for the jth tooth is written as

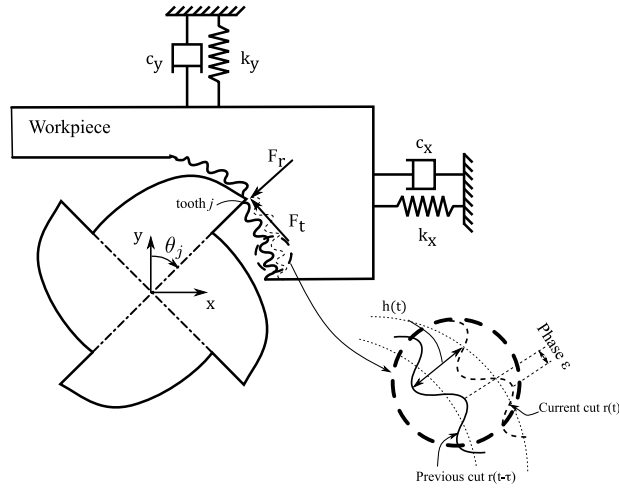$$h(t) = f_t \sin(\phi) + r(t - \tau) - r(t) \qquad\qquad (2)$$

Fig. 1. Schematic view for regenerative chatter in milling operation [51].

where $r(t)$ and $r(t - \tau)$ are the displacements of the workpiece where tool tip engages in the radial (r) direction in the current and past passes. τ and f_t are the time delay and the feed per tooth. $r(t - \tau)$ and $r(t)$ are the functions of tool rotation (ϕ). The vibration projected onto the x- and y- axis is written

$$r = -x \sin(\phi) - y \cos(\phi) \tag{3}$$

and the cutting forces projected onto the x- and y- axes are

$$F_x = -F_t \cos(\phi) - F_r \sin(\phi), \qquad\qquad F_y = F_t \sin(\phi) - F_r \cos(\phi). \tag{4}$$

The cutting forces will only occur when the corresponding tooth is engaging with the workpiece. Therefore, the total cutting forces considering all teeth engagement can be expressed as

$$F_{x,total} = \sum_{j=0}^{N_t-1} F_{x,j} g(\phi_j), \qquad\qquad F_{y,total} = \sum_{j=0}^{N_t-1} F_{y,j} g(\phi_j) \tag{5}$$

where N_t is the number of teeth and $g(\phi_j)$ is the switching function indicating tool engagement ($g(\phi_j) = 1$ if $\phi_s \leq \phi_j \leq \phi_e$; otherwise, $g(\phi_j) = 0$). Substituting Eqs. (1) to (4) into Eq. (5) yields

$$\begin{bmatrix} F_{x,total} & F_{y,total} \end{bmatrix}^T = \frac{1}{2} a K_t [A] [\Delta x \; \Delta y]^T \tag{6}$$

where $\Delta x = x(t) - x(t - \tau)$ and $\Delta y = y(t) - y(t - \tau)$, which can be expressed in the frequency domain as

$$\{\Delta(\omega)\} = \left(1 - e^{-i\omega\tau}\right) G(\omega) F_{total}(\omega), \tag{7}$$

and $[A]$ is time-varying milling force coefficients matrix:

$$[A(\omega_{tooth})] = \begin{bmatrix} a_{xx}(\omega_{tooth}) & a_{xy}(\omega_{tooth}) \\ a_{yx}(\omega_{tooth}) & a_{yy}(\omega_{tooth}) \end{bmatrix}, \tag{8}$$

which is a periodic function of tooth passing frequency (ω_{tooth}).

For the stability analysis, substituting Eq. (7) into Eq. (6) and rearranging it, the characteristic equation can be expressed as

$$\det\left([I] - \frac{1}{2} K_t a \left(1 - e^{-i\omega_c\tau}\right) [A] [G(\omega)]\right) = 0 \tag{9}$$

where ω_c and $G(\omega)$ are the chatter frequency and the frequency response function of the milling system. Solving Eq. (9) is not straightforward due to the time-dependency of $[A]$. To analytically solve this equation, the zero-order approach by Budak and Altintas [52] expands the time-varying force coefficient matrix into a Fourier series and takes only the constant term into consideration. The time-varying milling force coefficient matrix $[A]$ can be expanded into a Fourier series as

$$A(t) = \sum_r [A_r] e^{ir\omega_{tooth}t}, \tag{10}$$

where

$$[A_r] = \frac{1}{\tau} \sum_n \int_0^T \begin{bmatrix} a_{xx,n} & a_{xy,n} \\ a_{yx,n} & a_{yy,n} \end{bmatrix} e^{-in\omega_{tooth}t} dt. \tag{11}$$
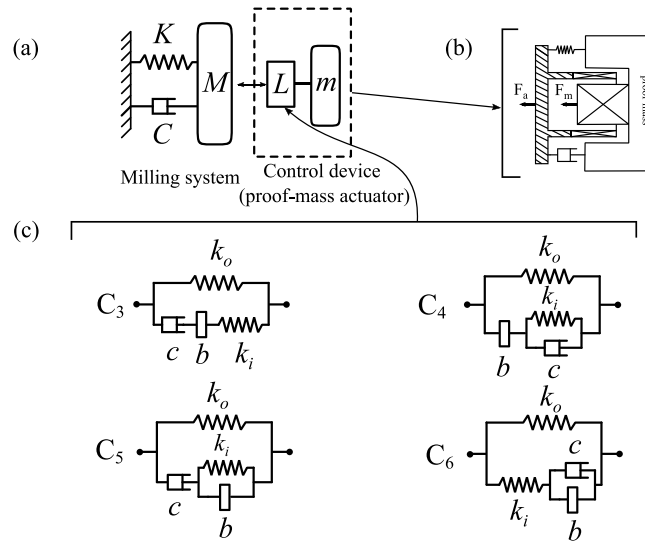
Fig. 2. (a) A SDOF milling system controlled with a proof mass actuator, as shown in (b), representing (c) four passive inerter-based configurations with a spring (k_o), and an inerter network consisting of a spring (k_i), a damper (c) and an inerter (b). L represents the IDVA configurations in (c), which is represented by the controller of the proof mass actuator in (b).

Considering only the constant term A_0 transforms time-varying terms in $[A]$ into averaged time-invariant term so that it allows an analytical solution to be obtained. This approach is a widely recognised, fast, and accurate analytical method [53], which is utilised in the present investigation. Considering a SDOF structure in milling with the assumption that the structure is rigid in the $x-$ direction ($\Delta x = 0$), the stability limit can be expressed [51]

$$a_{\lim} = \frac{2\pi}{a_{yy} N_t K_t Re\left[G_y\left(i\omega_c\right)\right]} \tag{12}$$

where a_{yy} is directional coefficient in the y-direction, which is derived from the single frequency solution of the dynamic milling coefficient matrix. The relationship between spindle speed and chatter frequency can be expressed as

$$N + \epsilon/2\pi = \omega_c \tau \tag{13}$$

where N and ϵ are the integer number of oscillations between subsequent tooth passes and the phase of the oscillations, respectively. All parameters in Eq. (12) are related to milling parameters except for the milling system's FRF $G_y\left(i\omega_c\right)$. The critical depth of cut $a_{\lim}$ is determined by the most positive or negative part of $G_y\left(i\omega_c\right)$, depending on the sign of a_{yy}. It is worth noting that the method presented here is identically applicable for negative values of a_{yy}. Depending on the directional coefficient, the most negative or positive real part determines the critical limiting depth of cut (absolute stability), below which the cutting is stable regardless of the spindle speed. This paper will focus on the case where a_{yy} is positive; therefore, the most negative real part of $G_y\left(i\omega_c\right)$ to improve the absolute stability limit.

2.2. Inerter-based dynamic vibration absorber

The milling system is modelled with a damped SDOF system as depicted in Fig. 2(a). It is controlled with an inerter-based dynamic vibration absorber, which is represented by a proof-mass actuator through an active control approach in this paper. Four layouts, referred to as IDVA-C3, IDVA-C4, IDVA-C5 and IDVA-C6 in Ref. [25], are illustrated in Fig. 2(b). The damped SDOF in Fig. 2(a) represents the milling system subjected to cutting forces and has parameters: mass M kg, stiffness K N/m, and viscous damping C N s/m. The inerter-based layouts are attached to the milling system to suppress chatter. Each layout is created by replacing the damper element in a TMD with an inerter network consisting of an inerter b kg, a spring k_i N/m and a viscous damper c N s/m. It also includes parameters for another spring k_o N/m and an auxiliary mass m kg.

The equations of motion of the SDOF system controlled with the IDVA, as shown in Fig. 2, are written in the Laplace domain as

$$M s^2 Y(s) + C s Y(s) + K Y(s) = F(s) + F_a(s), \tag{14}$$

where $F(s)$ and $F_a(s)$ are the cutting force and control force:

$$F_a(s) = m s^2 = L(s)\left(Y_a(s) - Y(s)\right), \tag{15}$$

where Y, Y_a and ω are the displacements of the main mass and auxiliary mass, and the excitation frequency, respectively. $L(s)$ is the mechanical impedance of the IDVA in the Laplace domain, which gives the control force as being proportional to the relative

Table 1
Structural parameters and milling parameters used in the optimisation and the stability lobed diagram.

Structural parameters			
Natural frequency	Stiffness		Damping ratio
129.29 Hz	1.34×10^7 N/m		1.34%

Milling parameters				
Milling type	Radial immersion	Number of teeth	Tangential cutting stiffness K_t	Radial cutting stiffness K_r
Down milling	Half immersion	4	660×10^6 N/mm^2	180×10^6 N/mm^2

Table 2
Optimal design parameters for the dynamic properties in Table 1 and $\mu = 0.0055$.

	γ	ζ	δ	η
TMD	1.0325	0.0473	–	–
IDVA$_{C3}$	1.0404	0.0427	0.0146	1.0030
IDVA$_{C4}$	1.0440	0.0012	0.0144	0.9916
IDVA$_{C5}$	1.0188	0.0518	2.1760	1.0985
IDVA$_{C6}$	1.0367	0.0012	0.0142	1.0147

displacement. The transfer function of the SDOF system controlled with the IDVA is written as

$$G(s) = \frac{Y(s)}{F(s)} = \frac{1/M}{s^2 + 2\zeta\omega_n s + \omega_n^2 + \frac{L(s)}{M}} \tag{16}$$

where $\omega_n = \sqrt{K/M}$ is the natural frequency of the milling system, $\zeta = C/(2\sqrt{MK})$ is the damping ratio of the milling system, and $L(s) = F_a Y(s)$ is the mechanical impedance of the control system, which is provided in Appendix A for each layout. In addition to the natural frequency ω_n and the damping ratio ζ_m, a series of non-dimensional parameters are defined to derive the non-dimensional transfer function: mass ratio $\mu = m/M$, inertance-to-mass ratio $\delta = b/m$, auxiliary damping ratio $\zeta_a = c/(2\sqrt{mk_o})$, corner frequency ratio $\eta = \omega_b/\omega_m$, natural frequency ratio $\gamma = \omega_m/\omega_n$, and $\lambda = \omega/\omega_n$, where $\omega_m = \sqrt{k_o/m}$ and $\omega_b = \sqrt{k_i/b}$. Using the non-dimensional parameters and substituting $s = i\omega$, a non-dimensional transfer function can be written in the frequency domain as follows:

$$\tilde{G}(\lambda, \gamma, \zeta_a, \delta, \eta, \zeta_m, \mu) = \frac{R_n + iI_n}{R_d + iI_d}. \tag{17}$$

Complete expressions for R_n, R_d, I_n, and I_d in Eq. (17) for each layout are provided in Appendix A. In the following section, the dimensionless FRFs derived in Eq. (17) are employed in the numerical optimisation to initially obtain the optimal dimensionless design parameters for a known mass ratio μ and the milling system's damping ratio ζ_m. Subsequently, the dimensional design parameters are determined for the identified dynamic structural properties.

3. Performance evaluation for absolute chatter stability

3.1. Numerical evaluation

The focus of this study is to improve the absolute stability limit and thus, the most negative real part of transfer function in Eq. (17) is considered in the optimisation problem. To obtain the optimal design parameters for the TMD and IDVAs, the self-differential evaluation algorithm [54] was utilised to minimise the objective function:

$$\max_{\gamma, \zeta_a, \delta, \eta} \left(\min_{\lambda} \left(\text{Re}\left(\tilde{G}(i\lambda)\right) \right) \right). \tag{18}$$

The damping ratio of the milling system was chosen as $\zeta_m = 1.34\%$ as identified from the experimental setup, which will be discussed in Section 3.2. The dynamic structural properties and the milling parameters utilised in the numerical performance evaluation are given in Table 1. These are the same values that were identified from the experimental setup for the most flexible part (the workpiece-beam-actuator system) so that the experimental validation of these numerical simulations was possible in the same experimental setup. The optimal dimensionless design parameters for $\mu = 0.0055$ are presented in Table 2. The small mass ratio was intentionally chosen based on numerical simulations to prevent actuator saturation during the experimental validation phase. This value is defined by the behaviour of the FRFs near resonance region. In the numerical analyses, the actuator forces were evaluated for whether they reach the actuator force limit for a range of depth of cuts and spindle speeds corresponding to the resonance region in the FRF, which predominantly referred to the lobing effect region in the SLDs. Therefore, higher values than the chosen mass ratio would lead to a saturation in the actuator for some depth of cuts and specific spindle speeds. To validate the absolute stability limit, the spindle speeds and depth of cuts in the validation tests presented in Section 3.2 were chosen from the safe regions (where lower actuator forces occur) as an extra precaution to avoid the actuator saturation.

For the properties in Table 1 and the optimal parameters in Table 2, the real values of FRFs for TMD and IDVAs are presented in Fig. 3(a). Using the FRFs, the SLDs obtained are demonstrated in comparison to the uncontrolled structure in Fig. 3(b). Due to
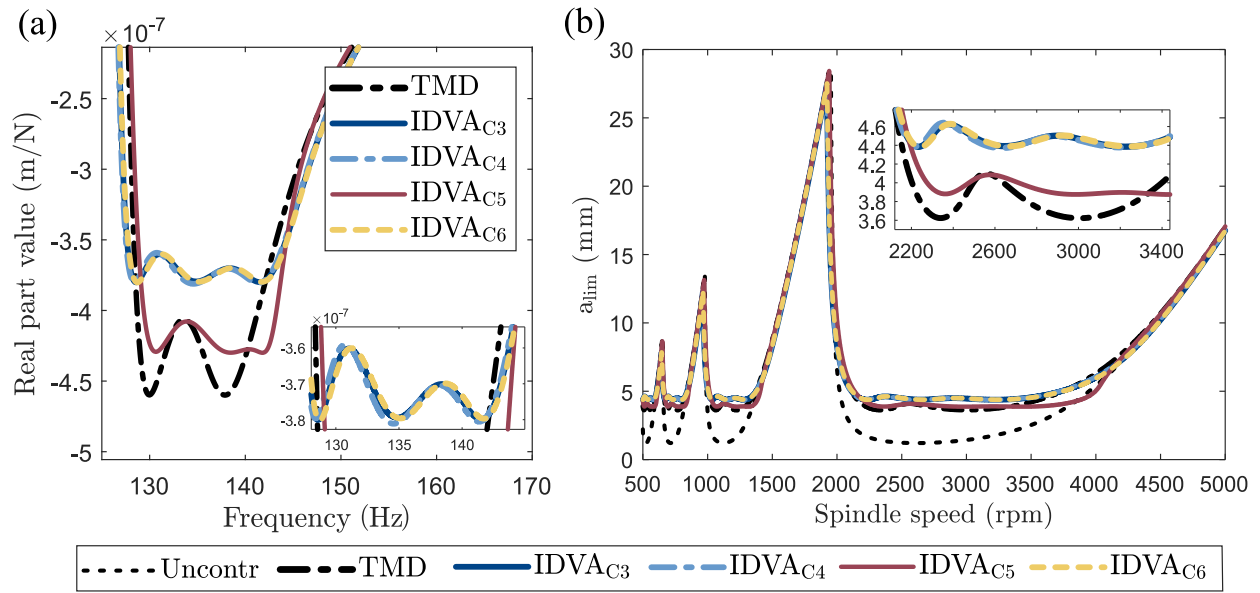
Fig. 3. (a) Real values of FRFs for the TMD and the IDVAs for the optimal parameters in Table 2, and (b) the SLDs obtained from the FRFs in comparison to the uncontrolled structure.
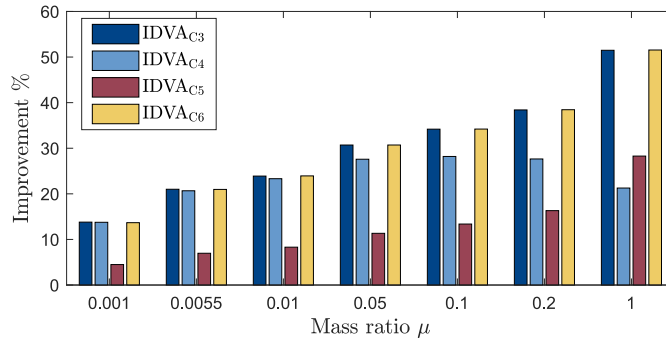

Fig. 4. Performance improvement in the absolute stability limit for the IDVAs compared to a classical TMD.

the increase in the most negative real part values of IDVAs compared to the TMD, all IDVAs improved the absolute stability limit in the SLD. The absolute stability limit, which was 1.2 mm for the uncontrolled structure, increased to 4.38 mm, 4.37 mm, 3.88 mm and 4.38 mm for IDVAs C3, C4, C5 and C6, respectively. Considering the critical depth of cut of 3.62 mm in the case of the TMD, the use of IDVA improved the absolute stability limit by $8 - 21\%$ for $\mu = 0.0055$.

The optimal design parameters for a selection of mass ratios μ $(0.001, 0.0055, 0.01, 0.05, 0.1, 0.2,$ and $1)$ were also determined to examine the performance improvement for different mass ratios. Fig. 4 shows absolute stability increment compared to the TMD for all mass ratios evaluated. All IDVAs except IDVA-C4 increased their relative performance in comparison of the TMD with the increasing mass ratio. The maximum performance improvement was around 14% when $\mu = 0.001$ and reached to just above 50% when $\mu = 1$ for both IDVA-C3 and IDVA-C6. For small mass ratios for IDVA-C4, the improvements were comparable with IDVA-C3 and IDVA-C6 while it started to lose its effectiveness for the higher values of the mass ratio than 0.1. This is in agreement with the vibration suppression performance of IDVA-C4 for H_∞ optimisation presented by Hu and Chen [25]. Its effectiveness compared to other IDVA layouts decreases with increasing mass ratios. It is worth pointing out that the improvements in Fig. 4 are given in comparison with the TMD, which can be virtually applied as VPA. This means that the performance of the IDVAs increase even more compared to the uncontrolled case as the TMD performance also increases with the increasing mass ratio.

3.2. Experimental verification

The experimental setup to verify the numerical results obtained is illustrated in Fig. 5. The stiffness of the workpiece setup was highly reduced in the $y-$direction by using a flexure, where the Al-7075 T6 material with the dimension of $(100 \times 100 \times 300 \text{ mm}^3)$ was fixed. Its stiffnesses in $x-$ and $y-$ directions were identified as 3.79×10^9 N/m and 1.34×10^7 N/m, respectively. The inertial
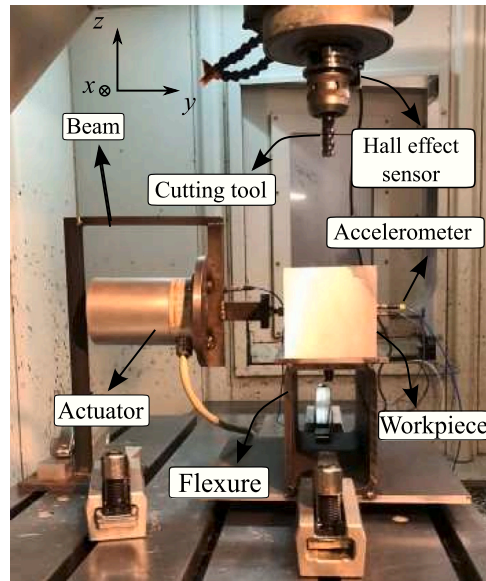
Fig. 5. Experimental milling setup consisting of a flexible workpiece system, an actuator supported by a beam, an accelerometer on the workpiece and a hall effect sensor.

actuator was attached to the workpiece through a beam to support the flexible direction. An accelerometer (PCB 353B18) and a hall effect sensor were utilised to measure the acceleration of the workpiece and the spindle speed, respectively. The acceleration data was utilised as the feedback data so that the actuator produced the same actuation force virtually acting as a passive IDVA device. The data was collected and processed by NI DAQ USB-4431. The collected acceleration data was analysed by applying the fast Fourier Transform (FFT) for the chatter detection. The milling experiments were conducted with the feed of 0.05 mm/tooth using a 4-tooth cutting tool with the diameter of 16 mm. The same milling parameters as listed in Table 1 were used for all experiments. Table 1 also indicates the dynamic properties of the workpiece system and the specific cutting stiffness identified. It should be noted that the tool's dominant natural frequency was also identified much higher than ($f_{n,tool} > 4000$ Hz) the workpiece's dominant natural frequency.

The controller was developed following the IDVA-C3 layout formula outlined in Appendix A. The workpiece's acceleration was acquired as the primary input for the control system. Converting the acceleration data yields the velocity and displacement of the workpiece. The control system parameters were fine-tuned for $\mu = 0.0055$. The control system generated an input value in the form of a voltage signal for the actuator. The actuator, in response to the magnitude of the acceleration, transformed this voltage output from the control system into a control force. The actuator shows a linear behaviour for the frequency of interest by producing 3 N per voltage [37].

The actuation force was provided by the proof-mass actuator with a maximum force capability of 27 N. The maximum actuation force was the primary limitation for selecting a small mass ratio, which prevents actuator saturation. In numerical evaluations, IDVA-C3 and IDVA-C6 performances were comparable to each other and superior to the others. Experiments were conducted for the validation of these most promising numerical evaluations.

The cutting tests were conducted to verify the chatter stability limits for uncontrolled and controlled cases. In the controlled case, the actuator was utilised to represent the IDVA device and only IDVA-C3 was examined for the validation. Fig. 6 demonstrates the experimental results with the predicted stability lobe diagrams. Firstly, the tests for the uncontrolled cases where the absolute stabilty limit was predicted to be 1.2 mm were performed. The cuts with axial depth of cuts of 2 mm at 700 rpm and 1100 rpm were verified as chatter. These spindle speeds were chosen deliberately to capture the largest unstable lobes. Then, the experiments were conducted for the controlled IDVA-C3 case. In order to verify the control effect on the absolute stability limit, a series of depth of cuts at 1100 rpm was examined until reaching the chatter. The once-per-revolution and FFT spectrum for these cuts that were used for the chatter detection are given in Appendix B. The depth of cuts of 4 mm and 5 mm indicated stable and marginal cuts, respectively. The chatter was observed for 6 mm depth of cut. The stability for 4 mm depth of cut was also verified with the cutting tests at 700 rpm, 800 rpm, and 900 rpm. Having considered that the 2 mm depth of cut caused chatter for the uncontrolled case, the absolute stability limit was improved with the IDVA-C3 as predicted from the stability lobe diagrams.

All the experimental results in Fig. 6(a) were conducted using an uncut Aluminium workpiece with subsequent cuts. Also, the total material removal for all experiments was small compared to the total mass of the workpiece. Therefore, it can be assumed that the change in dynamic properties initially identified was negligible. However, it is known that varying dynamic properties due to change in the clamping conditions and/or material removal can be an issue and it can cause a detuning effect on the IDVA optimal design parameters as is also the case for the TMD. To test this, further cutting tests were carried out by changing the dynamic
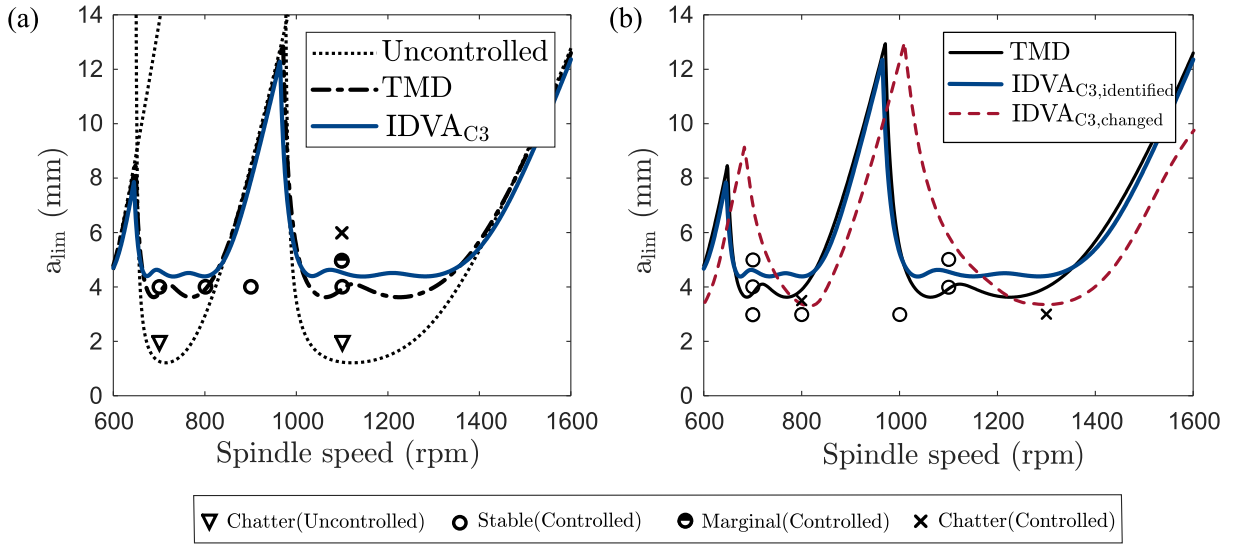
Fig. 6. (a) Predicted SLD for the dynamic properties in Table 1 for the uncontrolled case, the TMD, and the IDVA-C3 where the cutting tests are marked for the IDVA-C3. (b) Exploratory cutting tests conducted in comparison with the predicted SLDs obtained by initially identified and updated dynamic properties for the IDVA-C3.

Table 3
The mean and standard deviation values for normally distributed dynamic properties used in Monte Carlo simulation.

	K (kN/m)	f_n (Hz)	ζ_m
Mean (μ_{mean})	1340.3	129.29	0.0134
Standard deviation (σ)	$0.2\mu_{K,mean}$	$0.01\mu_{f_n,mean}$	$0.2\mu_{\zeta_m,mean}$

properties. For this, the workpiece used for previous set of experiments was replaced with a workpiece from which more material had been removed (so its mass is smaller), and the clamping conditions were slightly changed. With the new workpiece setup, the dynamic properties were identified: the natural frequency of 132.24 Hz, the stiffness of 1.22×10^7 N/m, and the damping ratio of 0.0146. The experimental results conducted by this setup are presented with the introduction of new dynamic properties in Fig. 6(b). As shown in the figure, the experimental results differ from the previous predicted SLD for the cutting tests conducted at 700 rpm, 800 rpm, 1100 rpm and 1300 rpm.

To illustrate the impact of the parameter variations more directly, if the stiffness is reduced by 15.7% to 1.13×10^7 N/m, then the controller becomes so de-tuned that the performance only matches that of the uncontrolled system, in terms of the absolute stability limit. This example and the results in Fig. 6(b) where all three dynamic parameters were changed indicates that the IDVA tuned for a specific set of dynamic properties loses its effectiveness with the deviation in the dynamic parameters. Although the adjustment of the design parameters is possible with the active control approach, this requires the identification of system parameters during cutting. Even if the dynamic properties remain unchanged, uncertainties in the system identification can still cause similar problems for the virtual passive absorber approach. Therefore, robustness analysis is important for a comprehensive investigation such a method, which will be presented next.

4. Robustness

The effectiveness of the passive absorbers, or virtual passive absorbers as proposed in this paper, is highly dependent on their robustness to changes in the dynamic properties of the primary systems. To evaluate the robustness of IDVAs in comparison to the TMD, a Monte Carlo simulation in the frequency domain was conducted by randomly generating input parameters and observing their effect on the stability limits. Uncertainty to the dynamic properties of the primary system (K, f_n and ζ_m) was applied using a latin hypercube sampling method [55] to ensure a fair representation of the input parameter space. 500 samples were generated and a normal distribution was applied to each input parameter. The mean values were set to the identified values presented in Table 1. The mean values and standard deviations are given in Table 3. In this analysis, the stability limit (or SLD) is considered as the output, applying Eq. (12). It is also assumed that the mass ratio is chosen such that no actuator saturation occurs even at the maximum actuator force.

The results of the uncertainty analysis conducted for the TMD and the four IDVAs are evaluated with the mean value and standard deviation for each spindle speed and each layout. The results are presented as the 95% confidence interval in the SLD form as well
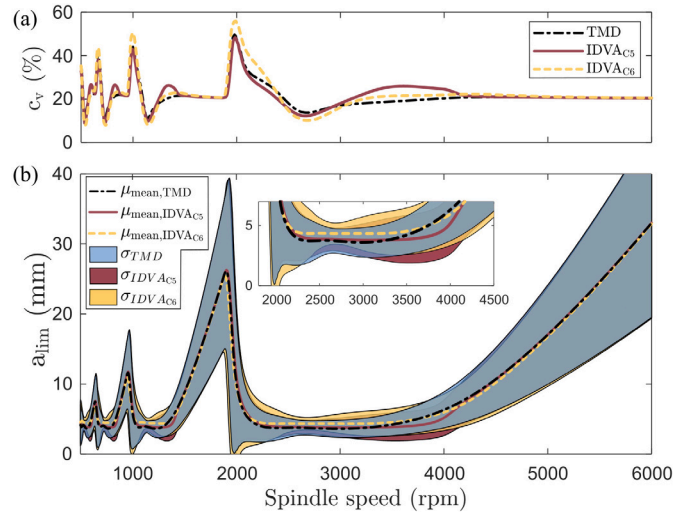
Fig. 7. (a) Coefficient of variance (cv) in percentage and (b) distribution of the stability limit for $\mu = 0.0055$ for the TMD, the IDVA C5, and IDVA C6 after running Monte Carlo simulation with uncertainties. Each curve and the filled region indicate the mean value and 95% confidence interval, respectively.

as coefficient of variance (CV) in percentage, which is the ratio of the standard deviation to the mean value:

$$c_{\mathrm{v}} = \frac{\sigma}{\mu_{mean}} \times 100. \tag{19}$$

As the SLD consists of repetitive scaled lobes of the same lobe, the focus is mostly on the zeroth lobe in the presented figures for a clear visualisation. The results for $\mu = 0.0055$ indicated that the mean values and the standard deviations are very close for IDVA-C3, C4 and C6. Among them, IDVA-C6 is slightly more robust than other two layouts as can be seen in Appendix C. Therefore, the rest of this section will focus on the comparison of the TMD, IDVA-C5, and IDVA-C6.

Fig. 7 demonstrates the coefficient of variance and 95% confidence interval along the spindle speed for the TMD, IDVA-C5 and IDVA-C6 for $\mu = 0.0055$ when three input parameters are varying. The results can be considered in three regions: the lobing effect region (1500–2000 rpms), the absolute stability region (2350–3000 rpms), and ultra-high speed region (after 4000 rpm). All absorbers show high variance in the lobing effect region. IDVA-C5 demonstrates a comparable coefficient of variance to the TMD while IDVA-C6 performs worse than the TMD. In the absolute stability region, both IDVAs outperform the TMD robustness having the coefficient of variances of 13.8%, 12.4% and 10.2% at 2700 rpm for the TMD, the IDVA-C5 and IDVA-C6, respectively. In between the absolute stability region and ultra-high speed region, both IDVAs have higher values than the TMD. IDVA-C5 shows the worst robustness in this region compared to other two absorbers. The coefficient of variance values get closer to each other as the spindle speed increases in the ultra-high speed region.

As the standard deviations are normalised by the mean values in Fig. 7(a), the increment provided by each absorber is not taken into account. In terms of that, Fig. 7(b) gives a better picture with the inclusion of the improvements. The lower boundaries of the filled areas in the figure indicate the guaranteed stability limit with a 95% confidence for the uncertainties considered. For instance, even though the TMD and the IDVA-C6 have the same coefficient of variance at 3057 rpm, the IDVA-C6 provides higher stability limit (considering the lower boundaries of the confidence interval) with the depth of cut 2.83 mm compared to 2.36 mm provided by the TMD. Also, it shows that the limiting depth of cut at 2700 rpm for the TMD is 2.69 mm whereas it is 3.46 for the IDVA-C6 with a 95% confidence. These spindle speeds chosen are close to spindle speed at which the absolute stability limit happens. These lower boundary values lead to a 28.6% increment in the stability limit, which is 7.6% higher than the improvement presented in Fig. 4 for the same mass ratio.

Fig. 8 presents the lower boundaries of 95% confidence interval for different mass ratios. The figure shows only the stable region, where the grey zone is always stable regardless of the use of any absorber from the TMD, IDVA-C5 or IDVA-C6. The further increment is shown with the colours for each absorber as indicated in the legend. It is clear from the figure that the best robustness in the lobing effect region and the transition from that zone to the absolute stability region is provided by the IDVA-C5, especially up to $\mu = 0.05$. The TMD shows a higher robustness towards ultra-high speed region. The absolute stability regions are mostly dominated by the IDVA-C6 for all the mass ratio values from 0.0010 to 0.2. Moreover, the dominance of the IDVA-C6 increases with the mass ratio. This is because of the increment in the improvement in this absorber compared to TMD.

Fig. 9 illustrates the results for the effects of uncertainty of only one parameter (K, f_n or ζ_m) on the stability limit for mass ratios of 0.0055 and 0.05 by keeping two other input parameters constant. The CVs for only varying K and f_n cases show similar behaviours to the CV in Fig. 7, where all input parameters vary. Unlike Fig. 7, the IDVA-C6 has better CV almost all spindle speeds in three regions including the lobing effect region compared to the TMD. The increase in the mass ratio slightly affected the CV for the case of K; however, it reduces the CVs for ζ_m and f_n. Therefore, higher mass ratio increases the robustness for the IDVAs as well as the TMD.
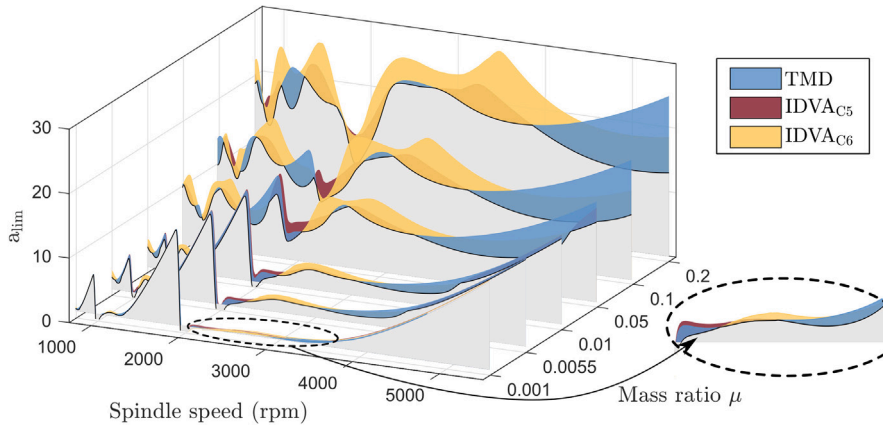
Fig. 8. Lower boundaries of the 95% confidence interval region given for TMD, IDVA-C5 and IDVA-C6 for different mass ratios. (For interpretation of the references to colour in this figure legend, the reader is referred to the web version of this article.)

The uncertainty analysis presented in this section evaluates relatively small variation in the natural frequency of the primary system. It is considered that high variation in the natural frequency can be addressed by adapting the parameters of the controller for estimated changes in the natural frequency (e.g., changes due to material removal). However, a case where the Monte Carlo simulation was run with the parameters in Table 3 but taking the standard deviation for the natural frequency as $0.1\mu_{f_n,mean}$ is presented in Appendix D as an extreme case.

5. Actuator saturation

Actuators have a limit on the maximum force that they can produce. When the control signal attempts to exceed this limit, the actuator becomes saturated, resulting in a failure to achieve the desired control performance. Hence, it is essential to consider actuator saturation effects in the control system. It is well-known that the higher the mass ratio, the higher the performance that can be achieved for a traditional TMD. However, for a virtual passive absorber approach, a high mass ratio leads to higher actuation forces that may not be achievable by an actuator. Therefore, actuator saturation is an important factor that limit the control system performance. The investigation of the actuator force for four IDVA layouts with a comparison of the TMD is considered in this section.

Rearranging the equations of motion in Eqs. (14) and (15), the transfer functions for the actuator force for the milling system are derived in the Laplace domain:

$$\frac{F_a(s)}{F(s)} = \frac{-L(s)ms^2}{\left(Ms^2 + Cs + K + L(s)\right)\left(ms^2 + L(s)\right) - L(s)^2} \tag{20}$$

where $L(s)$ is the mechanical impedance of the corresponding IDVA. Eq. (20) indicates the actuation force per unit cutting force. The cutting force in milling in y-direction, which is given in Eq. (6), is periodic at the tooth passing frequency due to the directional milling coefficient matrix $[A]$ as discussed in Section 2.

Considering the Fourier series expansion, the dominant harmonics of the cutting forces depend on the enter and exit angles of the cutting tools, and radial immersion. For high radial immersion, only a few harmonics are sufficient to characterise the cutting force with good accuracy. With a decrease in radial immersion, the repetitive milling force waveforms turn exceedingly narrow and intermittent, containing multiple harmonics when expressed in the form of Fourier series. The latter especially becomes important for the cases where the milling system is described by a multiple degree-of-freedom system as one of the harmonics can amplify the actuator force. Three important points considered in the analysis actuator force are:

- Due to the SDOF milling system studied in this paper and the relatively high spindle speed selected, it is assumed that the effects of higher harmonics, stemming from low radial immersion, on the actuator force will be limited.
- No helix angle for the cutting tool is considered for the sake of simplicity.
- Only steady-state response is examined.

The design parameters obtained in Section 3 were evaluated using Eq. (20) to account for the actuator saturation. The actuation FRF (F_a/F) for $\mu = 0.0055$ is presented in Fig. 10. The grey background indicates the frequency range corresponding to the lobing effect zone, and the dashed line marks the frequency at which the maximum stable depth of cut occurs. As a SDOF system is considered, the response is monotonic outside the frequency range presented in the figure. hh

In comparison to the TMD and IDVAs, significant differences in actuation forces only occur in the resonance region (120 Hz–160 Hz). Therefore, this frequency band is critical in the decision between one absorber to another in terms of actuation saturation. The tooth passing frequency or its harmonics that fall within this frequency range lead to an increase in the actuation force, mostly
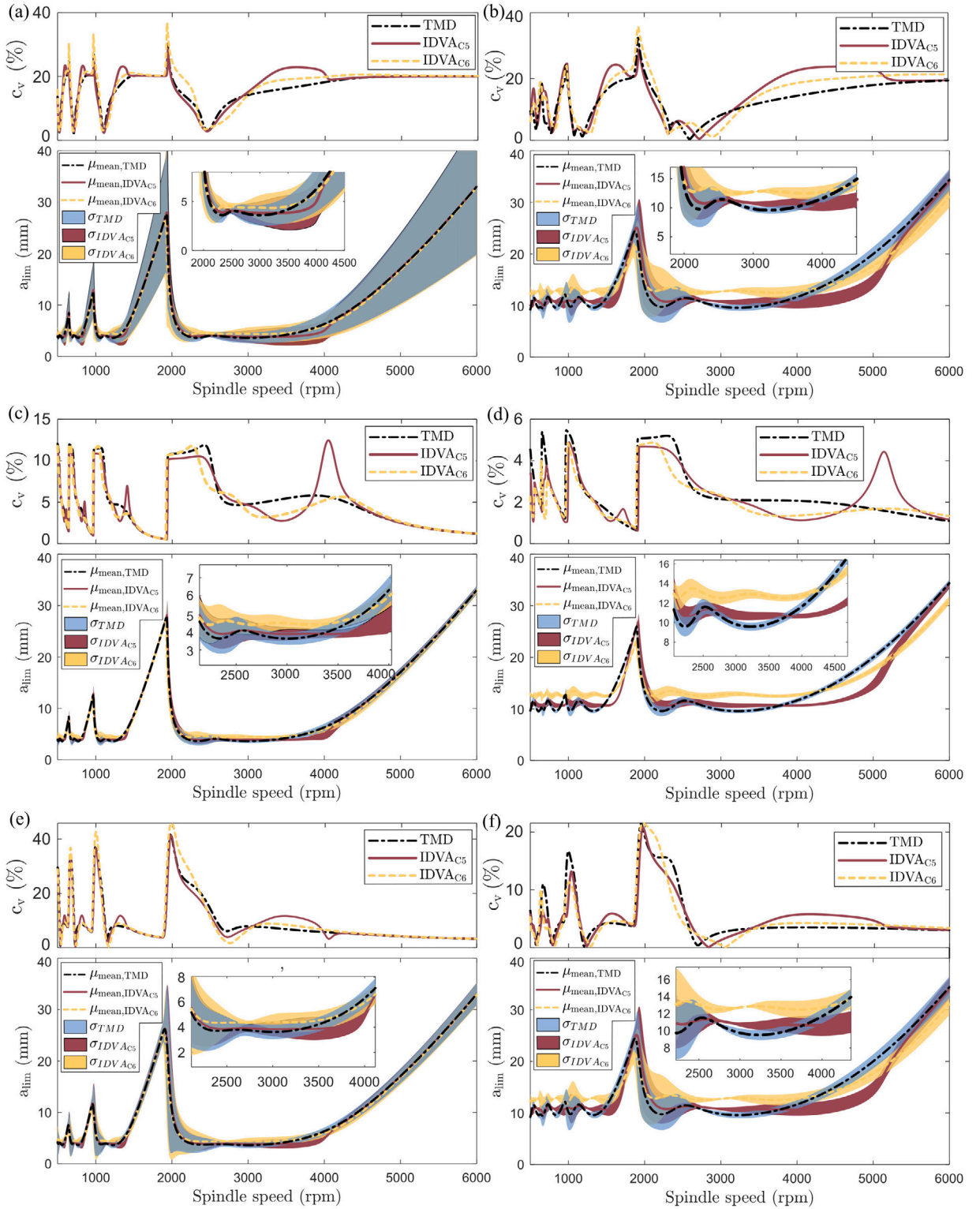
Fig. 9. Coefficient of variances (c_v) in percentage and distribution of the stability limit for TMD, IDVA-C5, and IDVA-C6 after running Monte Carlo simulation with uncertainties applied keeping all parameters the same except only one parameter: only stiffness (K) variable for (a) $\mu = 0.0055$ and (b) $\mu = 0.05$, only structural damping ratio (ζ_m) variable for (c) $\mu = 0.0055$ and (d) $\mu = 0.05$, and only natural frequency (f_n) variable for (e) $\mu = 0.0055$ and (f) $\mu = 0.05$.
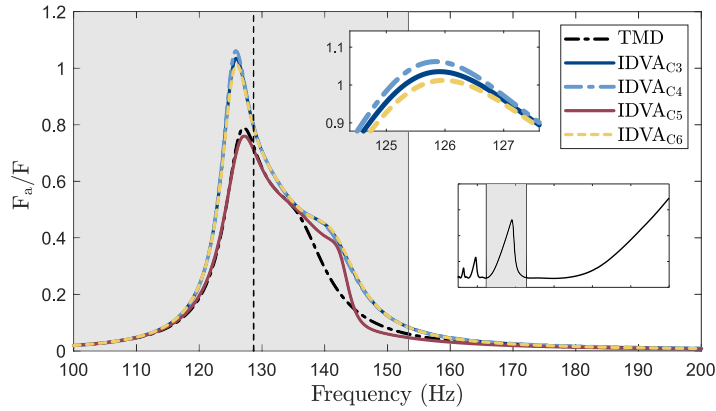
Fig. 10. The FRF for the actuation force per cutting force for $\mu = 0.0055$, where the black dash line indicates the tooth passing frequency(ω_{tooth}) referring to the spindle speed at which the maximum depth of cut occurs.

corresponding to the lobing effect zone. The TMD and IDVA-C5 produce lower actuator forces at all frequency ranges than the IDVA-C3, IDVA-C4 and the IDVA-C6. For the absolute stability zone, which is around 160 Hz for this particular case, and beyond of that zone, the actuation forces become very similar.

Since the actuation FRF in Fig. 10 is obtained for parameters optimised to maximise the absolute stability, it can be assumed that the primary interest for the working spindle speed lies in the absolute stability region. Therefore, the actuator forces in this region are the most important.

Fig. 11 presents the actuation FRFs for mass ratios of 0.0010, 0.01, 0.05 and 0.1 for all absorbers. As the mass ratio increases, although the maximum actuation forces still occur in the lobing effect zone, actuation forces differ in the absolute stability region. IDVA-C5 produces the lowest actuator force while the IDVA-C4 generates the highest actuator force when considering the maximum actuator forces. With the increasing mass ratio, IDVA-C6 approaches the TMD. For the frequency at which the maximum stable depth of cut occurs, the actuator forces become almost identical as the mass ratio increases. For the absolute stability region, the TMD performs lower actuator force, whereas IDVA-C6 produces higher actuator force for large mass ratios. The validation of the results presented in Figs. 10 and 11 was made through time-domain simulations [56] for both high and low immersion cuts and are given in Appendix E.

Actuator force with uncertainty

Uncertainties in the system parameters affect not only the stability limit but also the actuation force. Selecting the mass ratio and machining parameters to give the maximum actuator force possibly leads to actuator saturation due to uncertainties in these parameters. Using the same normally distributed system parameters obtained from the Monte Carlo simulation in Section 4, changes in the actuation forces with the uncertainty were analysed.

Fig. 12 shows the upper boundaries of 95% confidence interval for the actuator force at mass ratios of 0.0010, 0.0055, 0.05, and 0.1. The results are compared to actuator forces in ideal conditions, where no uncertainties are considered. Consequently, the values in the figures are normalised to the ideal actuator force. For the uncertainties considered, up to approximately a 1.5 fold increase for TMD and IDVAs is observed in the actuator force within the absolute stability region with 95% confidence. The maximum variation in the actuator force reaches 2.5 fold in the lobing effect region. Therefore, the mass ratio should be cautiously chosen to avoid actuator saturation caused by uncertain parameters.

Comparison of two equal peak methods

Thus far, optimal design parameters have been determined by applying equal peak method for the real part of the FRF, known as Sims' method [10]. This method maximises the absolute stability by minimising or maximising the real part values at the cost of higher maximum actuator forces. Considering the actuator force saturation, Den Hartog's method [57] might be more advantageous as it generally requires lower actuator forces. However, it is important to evaluate each method's effectiveness in the context of the specific system being analysed and the actuator's capabilities.

Den Hartog's and Sims' methods in the context of actuator saturation were compared for different mass ratios using the dynamic parameters and milling parameters in Table 1. All design optimal design parameters were determined via numerical optimisation. The maximum FRF for the actuator force and the minimum real part values of the FRFs are presented in Fig. 13. Each data point in the figure shows the mass ratio for which the maximum FRF for the actuator force and the real part values. As demonstrated in the figure, Sims' method results in higher maximum actuator forces compared to Den Hartog's method. This is expected because Den Hartog's method minimises the magnitude of the system, and the relative displacement between the main and auxiliary systems.
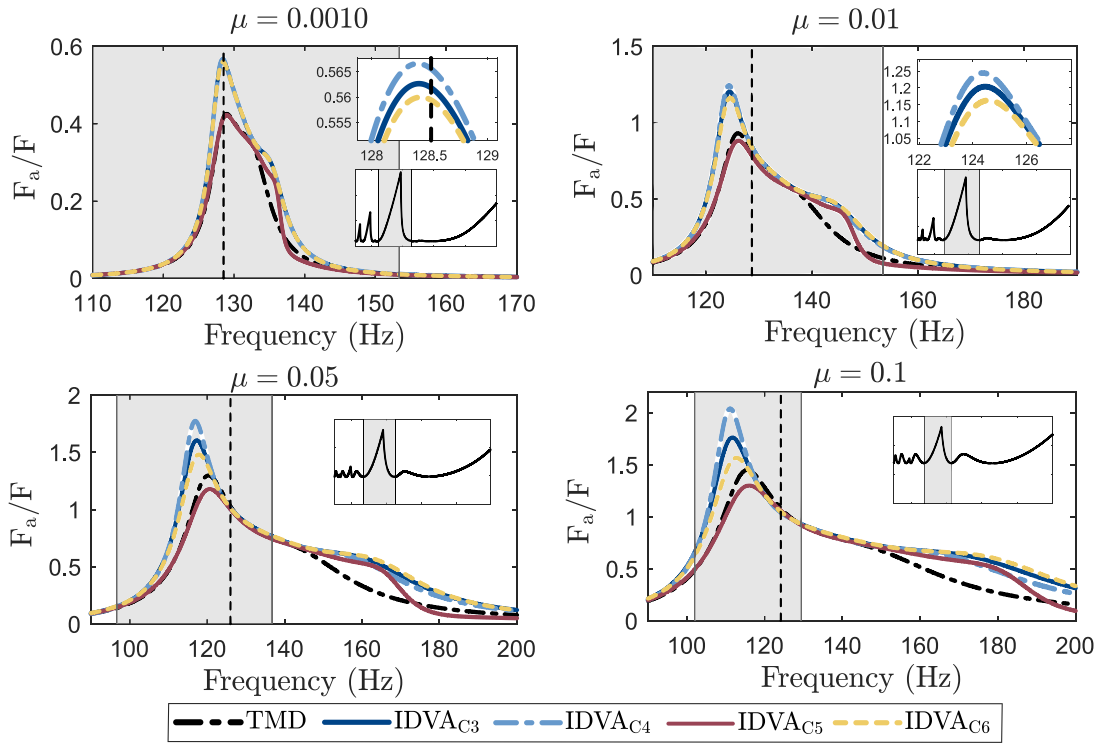
Fig. 11. The FRFs for the actuation force per cutting force for (a) $\mu = 0.0010$, (b) $\mu = 0.01$, (c) $\mu = 0.05$, and (d) $\mu = 0.1$.
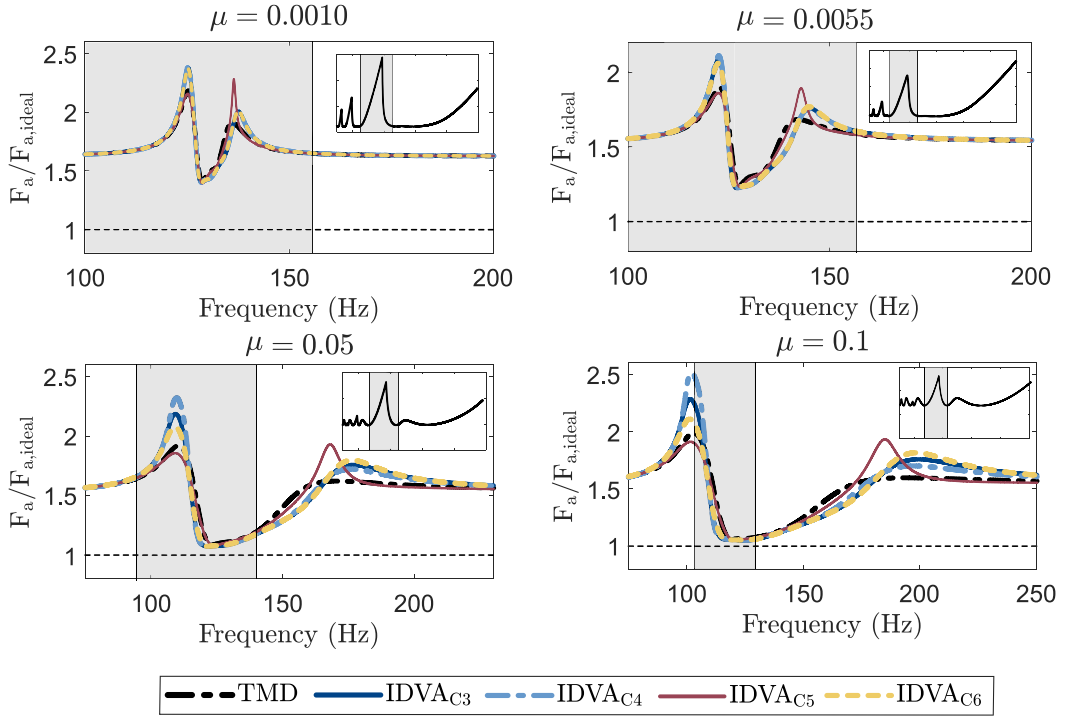

Fig. 12. The upper boundaries of 95% confidence interval for the normalised actuator force ($F_a/F_{a,ideal}$) for (a) $\mu = 0.0010$, (b) $\mu = 0.0055$, (c) $\mu = 0.05$, and (d) $\mu = 0.1$.
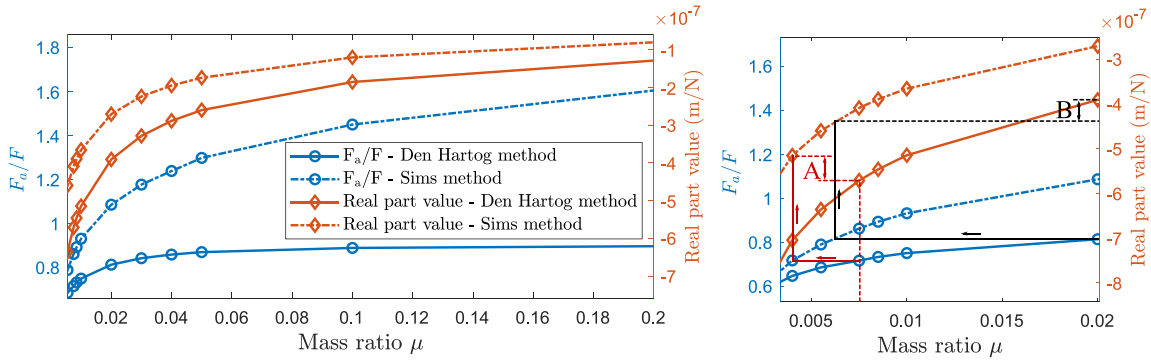
Fig. 13. (a) Actuation forces and real part responses for Den Hartog's and Sims' methods applied for different mass ratios. (b) The effects of two different methods on the real responses (A and B) are shown for two maximum actuation forces.

Although the Den Hartog's method leads to lower maximum actuator forces, it causes lower stability limit providing lower real part responses.

An example with two cases (A and B) is shown in Fig. 13(b). Assuming an unit cutting force and maximum actuator force of around 0.7 N, the mass ratio for Den Hartog's method can be chosen to be 0.075. The same actuator force for Sims' method is obtained with a smaller mass ratio, which eventually leads to higher stability limit by providing a higher negative real part response (as marked A). In the other case (case B), the mass ratio for Den Hartog's method is chosen to be 0.02, assuming a unit cutting force and maximum actuator force of around 0.8 N. The same actuator force for Sims' method requires a choice of a smaller mass ratio, which, this time, leads to lower stability limit by providing a smaller negative real part response. Two cases require different optimisation methods to obtain the best performance. However, this example considered only the maximum actuator forces, which occurs in the lobing effect region. The actuation FRFs presented in Figs. 10 and 11 provide smaller amplitudes outside the resonance region, so Sims' method becomes more effective again if the lobing effect will not be benefited. Therefore, there is a trade-off between Den Hartog and Sims' methods when the actuator saturation is involved. The decision of which method to use is case-specific.

6. Discussion

The analysis presented in this paper has clearly demonstrated that the virtual IDVA is more effective than the virtual TMD for active chatter control. Nonetheless, there are several aspects that merit additional discussion.

The virtual IDVA has provided all the benefits of the virtual TMD, but with superior performance and robustness. The active control approach offers the adaptability that can be useful for adjusting parameters in response to changes in dynamic parameters, such as natural frequency, due to the material removal and/or clamping conditions. Although changes due to material removal can be determined so that parameters can be adjusted, it is challenging to address deviations in system parameters identified in a static position in the operational mode during cutting. This issue has been investigated in this paper through the robustness analyses, showing that IDVAs provided a more robust solution. Even with material removal, determining changes in natural frequency can be difficult for complex structures. The robustness analysis provided for varying f_n is particularly interested, as the material removal introduces this type of uncertainty. Uncertainties in milling parameters such as specific cutting coefficients or immersion, have not been discussed because they act as a gain in the stability equation (as shown in Eq. (12)), making their importance less critical for a SDOF milling system. Therefore, the focus was on the uncertainties in the structural dynamic part of the equation. The uncertainty analysis conducted in this paper can also be viewed as an application of the digital twin concept. By simulating the impact of uncertainties on system performance, a virtual representation that helps anticipate and mitigate potential issues in real-world applications is created. This approach contributes to enhancing the adaptability and robustness of the virtual IDVA system.

It has been shown that the mass ratio influences performance and robustness similarly to that of the TMD. However, a high mass ratio is limited by the actuator saturation, which can lead to instability and performance degradation. The experimental setup has a high modal mass, making it difficult to achieve a high mass ratio. For smaller workpieces, higher mass ratios are possible, resulting in increased robustness and performance compared to classical TMDs. It is important to note that only steady-state responses were considered when assessing actuator force. Transient actuator forces, which initially occur in the time-domain response (as it appears in time domain response presented in Appendix E), might be worth considering to avoid saturation and instabilities.

Since passive absorbers do not have saturation problems, Sims' method provides the best performance for chatter suppression. However, for active systems involving an actuator, Den Hartog's method may be more preferable for parameter optimisation due to smaller actuator force generated. Moreover, the uncertain system parameters causes higher actuation force than the case where no uncertainty is considered. This further limits the performance improvement. Therefore, the choice of the optimisation method is case-specific, and an ad hoc optimisation method could potentially offer better results than Den Hartog's and Sims' methods. It should also be noted that a helical fluted tool will reduce the cutting forces and hence the actuator force. In this paper, only a SDOF system was considered; however, for complex structures with multiple degree-of-freedom, higher harmonics may trigger higher modes, particularly for low immersion cuts.

The focus of this study was on the absolute stability limit, assuming that the working spindle speed lies within that region of the SLD. Operating within the lobing effect region can result in higher actuator forces, especially for small mass ratios. If the working spindle speed of interest lies within the lobing effect region, a different optimisation approach with an objective function targeting performance maximisation for the lobing effect should be considered. It is also possible to use an approach by setting design parameters differently for various regions of the SLD.

Since the analysis was based on an experimental setup with structural damping, the optimal design parameters were found via numerical optimisation. For low structural damping, analytical solutions for Sims' and Den Hartog's methods can be directly utilised for the optimal design parameters.

Performance evaluation and robustness analysis presented in this paper are also applicable for passive devices. Robustness analysis can be particularly beneficial when applying these designs with passive control methods. However, the system's modal mass in machining operations is generally small, making the physical realisation of the IDVAs problematic because of the small inertance required. Also, realising this structure without introducing parasitic mass effects or extra stiffness can be a challenging task [27]. Therefore, the virtual IDVA method may be the most effective way to implement an ideal IDVA application for small mass ratios.

Considering the practical implementation of such virtual passive systems is important. While the experimental setup may seem impractical, its feasibility can be improved through approaches such as robotic assistance [37]. By employing an actively controlled robotic arm to support the workpiece, the proposed approach can be applied in machining application while maintaining the desired performance and robustness.

7. Conclusion

This paper has presented a comprehensive analysis of IDVAs for active chatter suppression with a focus on maximising the absolute stability limit. While the main objective was to determine the optimal design parameters for achieving absolute stability limit, evaluations were conducted across all regions of the SLD, including the lobing effect region, the absolute stability region, and ultra-high-speed zone. Based on the analysis, the following conclusions can be drawn:

- Performance evaluation of IDVAs compared to a classical TMD has been demonstrated with all IDVAs outperforming a classical TMD. The best performances are provided by IDVA-C3 and IDVA-C6 for all mass ratios, while IDVA-C4 performs well only for small mass ratios.
- The performance improvement was experimentally verified for IDVA-C3. Additionally, it was shown that varying dynamic parameters led to performance degradation with detuned design parameters.
- Robustness of IDVAs was assessed for the uncertainties in the main structure dynamic parameters through Monte Carlo simulation. The results indicate that IDVA-C3, IDVA-C4 and IDVA-C6 are more robust than the TMD and IDVA-C5. Their robustness increases with mass ratio. By combining robustness with performance improvement, IDVAs become increasingly preferable over a classical TMD in virtual passive absorber approach.
- The performance of the virtual IDVA approach is limited by actuator saturation. The actuator forces generated by each IDVA were first evaluated by neglecting uncertainties in the system parameters. The results revealed that actuator forces for IDVAs and the TMD differ in the lobing effect zone for small mass ratios. However, there is no significant difference in the actuator forces among IDVAs and the TMD for absolute stability region and beyond. Considering the uncertainties showed up to 1.5–2.5 fold increases in the actuator forces for all absorbers including the TMD.
- Unlike passive control methods, applying Sims' method may not be the best option to achieve optimal suppression performance due to high maximum actuator forces if actuator saturation is to be avoided across all spindle speeds with design parameters tuned for the absolute stability limit. In such cases, an ad hoc optimisation approach may be more desirable.

In conclusion, this study has demonstrated the potential advantages and application of IDVAs for active chatter suppression. Some of these techniques can also be applied to passive devices. However, there are some limitations and areas for future work to further enhance the performance and applicability of IDVAs. Future research could investigate the use of IDVAs for complex structures with multiple degree-of-freedom to broaden their applicability. Furthermore, examining additional sources of uncertainty, such as machining parameters, would help better understand their impact on IDVA performance and robustness. Investigating other optimisation objectives or incorporating multi-objective optimisation methods could lead to more versatile and robust IDVA implementations.

The works presented in [37,49,58] provided comparisons of the VPA with other traditional active control methods. The analysis in this study demonstrated that a virtual IDVA in an active control scheme is a better approach than the VPA. Therefore, it can be commented that a virtual IDVA will provide a better performance than all traditional control methods that are outperformed by the VPA. However, a direct comparison of the virtual IDVA with other traditional methods has been considered as the out of scope of this study. A full comparison of a virtual IDVA with other traditional methods has remained a separate work for future.

CRediT authorship contribution statement

Hakan Dogan: Conceptualization, Investigation, Methodology, Validation, Writing – original draft, Writing – review & editing. **Muhammet Ozsoy:** Conceptualization, Investigation, Validation, Writing – review & editing. **Erdem Ozturk:** Supervision, Writing – review & editing. **David J. Wagg:** Supervision, Writing – review & editing. **Neil D. Sims:** Supervision, Writing – review & editing.

Declaration of competing interest

The authors declare that they have no known competing financial interests or personal relationships that could have appeared to influence the work reported in this paper.

Data availability

Data will be made available on request.

Appendix A. Complete terms for frequency response functions

Mechanical impedances ($F_a = Ly(t)$) for the control device are presented in the Laplace domain as followings:

$$L_{IDVA_{C3}}(s) = k_o + \frac{bck_i s^2}{bcs^2 + (bs + c)k_i}$$

$$L_{IDVA_{C4}}(s) = k_o + \frac{b(cs + k_i)s^2}{bs^2 + cs + k_i}$$

$$L_{IDVA_{C5}}(s) = k_o + \frac{(bs^2 + k_i)cs}{bs^2 + cs + k_i}$$

$$L_{IDVA_{C6}}(s) = k_o + \frac{(bs + c)k_i s}{bs^2 + cs + k_i}$$

Complete terms in Eq. (17) are given as follows:

$$R_{n,IDVA_{C3}} = -2\delta\eta^2\gamma^2\lambda^2\zeta_a + 2\eta^2\gamma^4\zeta_a - 2\eta^2\gamma^2\lambda^2\zeta_a - 2\gamma^2\lambda^2\zeta_a + 2\lambda^4\zeta_a$$

$$I_{n,IDVA_{C3}} = \delta\eta^2\gamma^3\lambda - \delta\eta^2\gamma\lambda^3$$

$$R_{d,IDVA_{C3}} = 2\delta\eta^2\gamma^2\lambda^4\mu\zeta_a + 2\delta\eta^2\gamma^2\lambda^4\zeta_a - 2\eta^2\gamma^4\lambda^2\mu\zeta_a - 2\eta^2\gamma^4\lambda^2\zeta_a + 2\eta^2\gamma^2\lambda^4\zeta_a - 2\delta\eta^2\gamma^2\lambda^2\zeta_a$$
$$+ 2\gamma^2\lambda^4\mu\zeta_a + 2\eta^2\gamma^4\zeta_a - 2\eta^2\gamma^2\lambda^2\zeta_a + 2\gamma^2\lambda^4\zeta_a - 2\lambda^6\zeta_a - 2\gamma^2\lambda^2\zeta_a + 2\lambda^4\zeta_a$$

$$I_{d,IDVA_{C3}} = -\delta\eta^2\gamma^3\lambda^3\mu - \delta\eta^2\gamma^3\lambda^3 + \delta\eta^2\gamma\lambda^5 + \delta\eta^2\gamma^3\lambda - \delta\eta^2\gamma\lambda^3$$

$$R_{n,IDVA_{C4}} = -\delta^2\eta^2\gamma^2\lambda^2 + \delta\eta^2\gamma^4 - \delta\eta^2\gamma^2\lambda^2 - \delta\gamma^2\lambda^2 + \delta\lambda^4$$

$$I_{n,IDVA_{C4}} = -2\delta\gamma\lambda^3\zeta_a + 2\gamma^3\lambda\zeta_a - 2\gamma\lambda^3\zeta_a$$

$$R_{d,IDVA_{C4}} = \delta^2\eta^2\gamma^2\lambda^4\mu + \delta^2\eta^2\gamma^2\lambda^4 - \delta\eta^2\gamma^4\lambda^2\mu - \delta\eta^2\gamma^4\lambda^2 + \delta\eta^2\gamma^2\lambda^4 - \delta^2\eta^2\gamma^2\lambda^2$$
$$+ \delta\gamma^2\lambda^4\mu + \delta\eta^2\gamma^4 - \delta\eta^2\gamma^2\lambda^2 + \delta\gamma^2\lambda^4 - \delta\lambda^6 - \delta\gamma^2\lambda^2 + \delta\lambda^4$$

$$I_{d,IDVA_{C4}} = 2\delta\gamma\lambda^5\mu\zeta_a + 2\delta\gamma\lambda^5\zeta_a - 2\gamma^3\lambda^3\mu\zeta_a - 2\gamma^3\lambda^3\zeta_a + 2\gamma\lambda^5\zeta_a - 2\delta\gamma\lambda^3\zeta_a + 2\gamma^3\lambda\zeta_a - 2\gamma\lambda^3\zeta_a$$

$$R_{n,IDVA_{C5}} = \delta\eta^2\gamma^4 - \delta\eta^2\gamma^2\lambda^2 - \delta\gamma^2\lambda^2 + \delta\lambda^4$$

$$I_{n,IDVA_{C5}} = 2\delta\eta^2\gamma^3\lambda\zeta_a - 2\delta\gamma\lambda^3\zeta_a + 2\gamma^3\lambda\zeta_a - 2\gamma\lambda^3\zeta_a$$

$$R_{d,IDVA_{C5}} = -\delta\eta^2\gamma^4\lambda^2\mu - \delta\eta^2\gamma^4\lambda^2 + \delta\eta^2\gamma^2\lambda^4 + \delta\gamma^2\lambda^4\mu + \delta\eta^2\gamma^4 - \delta\eta^2\gamma^2\lambda^2 + \delta\gamma^2\lambda^4$$
$$- \delta\lambda^6 - \delta\gamma^2\lambda^2 + \delta\lambda^4$$

$$I_{d,IDVA_{C5}} = -2\delta\eta^2\gamma^3\lambda^3\mu\zeta_a - 2\delta\eta^2\gamma^3\lambda^3\zeta_a + 2\delta\gamma\lambda^5\mu\zeta_a + 2\delta\eta^2\gamma^3\lambda\zeta_a + 2\delta\gamma\lambda^5\zeta_a - 2\gamma^3\lambda^3\mu\zeta_a$$
$$- 2\gamma^3\lambda^3\zeta_a + 2\gamma\lambda^5\zeta_a - 2\delta\gamma\lambda^3\zeta_a + 2\gamma^3\lambda\zeta_a - 2\gamma\lambda^3\zeta_a$$

$$R_{n,IDVA_{C6}} = -\delta^2\eta^2\gamma^2\lambda^2 + \delta\eta^2\gamma^4 - \delta\eta^2\gamma^2\lambda^2 - \delta\gamma^2\lambda^2 + \delta\lambda^4$$

$$I_{n,IDVA_{C6}} = 2\delta\eta^2\gamma^3\lambda\zeta_a + 2\gamma^3\lambda\zeta_a - 2\gamma\lambda^3\zeta_a$$

$$R_{d,IDVA_{C6}} = \delta^2\eta^2\gamma^2\lambda^4\mu + \delta^2\eta^2\gamma^2\lambda^4 - \delta\eta^2\gamma^4\lambda^2\mu - \delta\eta^2\gamma^4\lambda^2 + \delta\eta^2\gamma^2\lambda^4 - \delta^2\eta^2\gamma^2\lambda^2$$
$$+ \delta\gamma^2\lambda^4\mu + \delta\eta^2\gamma^4 - \delta\eta^2\gamma^2\lambda^2 + \delta\gamma^2\lambda^4 - \delta\lambda^6 - \delta\gamma^2\lambda^2 + \delta\lambda^4$$

$$I_{d,IDVA_{C6}} = -2\delta\eta^2\gamma^3\lambda^3\mu\zeta_a - 2\delta\eta^2\gamma^3\lambda^3\zeta_a + 2\delta\eta^2\gamma^3\lambda\zeta_a - 2\gamma^3\lambda^3\mu\zeta_a - 2\gamma^3\lambda^3\zeta_a + 2\gamma\lambda^5\zeta_a$$
$$+ 2\gamma^3\lambda\zeta_a - 2\gamma\lambda^3\zeta_a$$

Appendix B. Once-per-revolution and frequency spectrum for experiments

Once-per-revolution and frequency spectrum for the experiments in Fig. 6(a) are presentedn in Fig. 14.

Appendix C. Comparison of robustness results of IDVA$_{C3}$, IDVA$_{C4}$ and IDVA$_{C6}$

Comparison of robustness results of IDVA$_{C3}$, IDVA$_{C4}$ and IDVA$_{C6}$ indicates that three IDVAs performs comparable robustness (see Fig. 15).
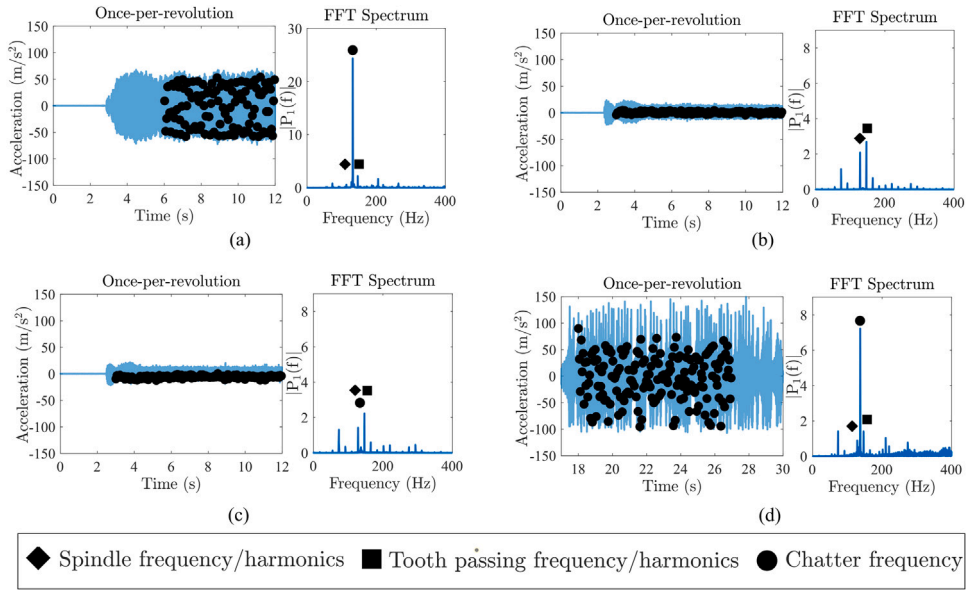
Fig. 14. Once-per-revolutions and frequency spectra for the cutting tests in Fig. 6(a): (a) uncontrolled, 1100 rpm, 2 mm depth of cut; (b) controlled, 1100 rpm, 4 mm depth of cut; (c) controlled, 1100 rpm, 5 mm depth of cut; (d) controlled, 1100 rpm, 6 mm depth of cut.
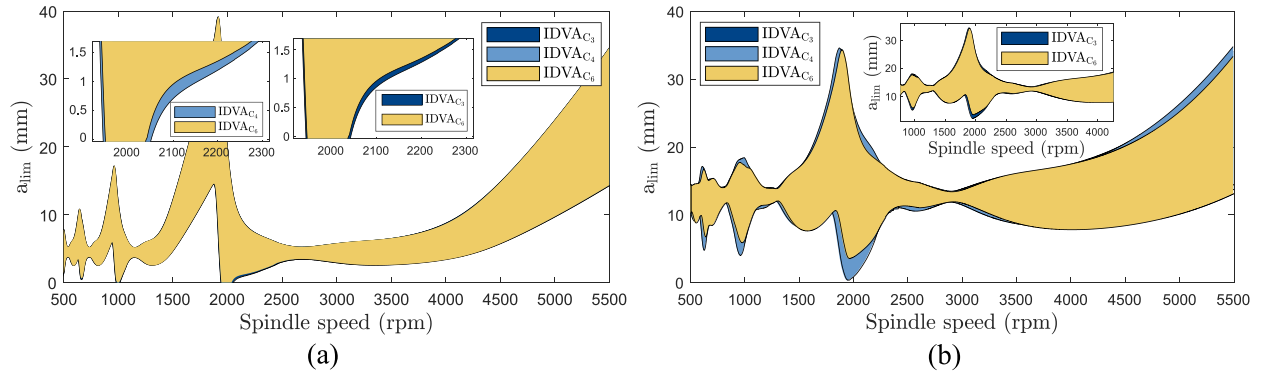

Fig. 15. Robustness of $IDVA_{C3}$, $IDVA_{C4}$ and $IDVA_{C6}$ for (a) $\mu = 0.0055$ and (b) $\mu = 0.05$.

Appendix D. Uncertainty analysis for high standard deviation for the natural frequency

The standard deviation for the natural frequency was considered as $0.1\mu_{f_n,mean}$ for mass ratio of 0.0055 to observe the effect of high variation from the nominal natural frequency. For the rest of the dynamic properties of the primary system was taken as presented in 3 and a Monte Carlo simulation was conducted for 500 samples for all four IDVA layouts and TMD. All SLDs are demonstrated in Fig. 16(a). Since the high variation in the natural frequency causes high shift in the location of the troughs in the SLD, it is not possible to obtain a meaningful results from the normal distribution of the results. Therefore, only the minimum stable depth of cut for each layout is presented in Fig. 16(b).

Appendix E. Time domain simulations for actuation forces

Time domain simulations were conducted to verify the actuation force results presented in Figs. 10 and 11. Parameters to obtain the time domain results in Fig. 17 are presented in Table 4. Milling parameters that are not given in Table 4 were taken from Table 1. The frequency spectrum of the cutting forces for two cases in Fig. 17(a) and (b) where consider both high and low radial immersions are also demonstrated in Fig. 17(c) and (d), respectively.
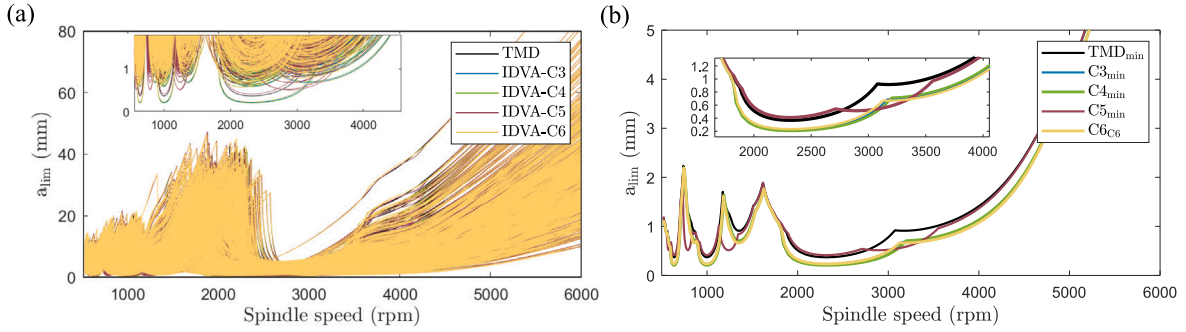
Fig. 16. (a) Monte Carlo simulation results for each IDVA and TMD for the mass ratio of 0.0055 and (b) the minimum stable depth of cut for each layout.

Table 4
Milling parameters for the time domain simulations presented in Fig. 17.

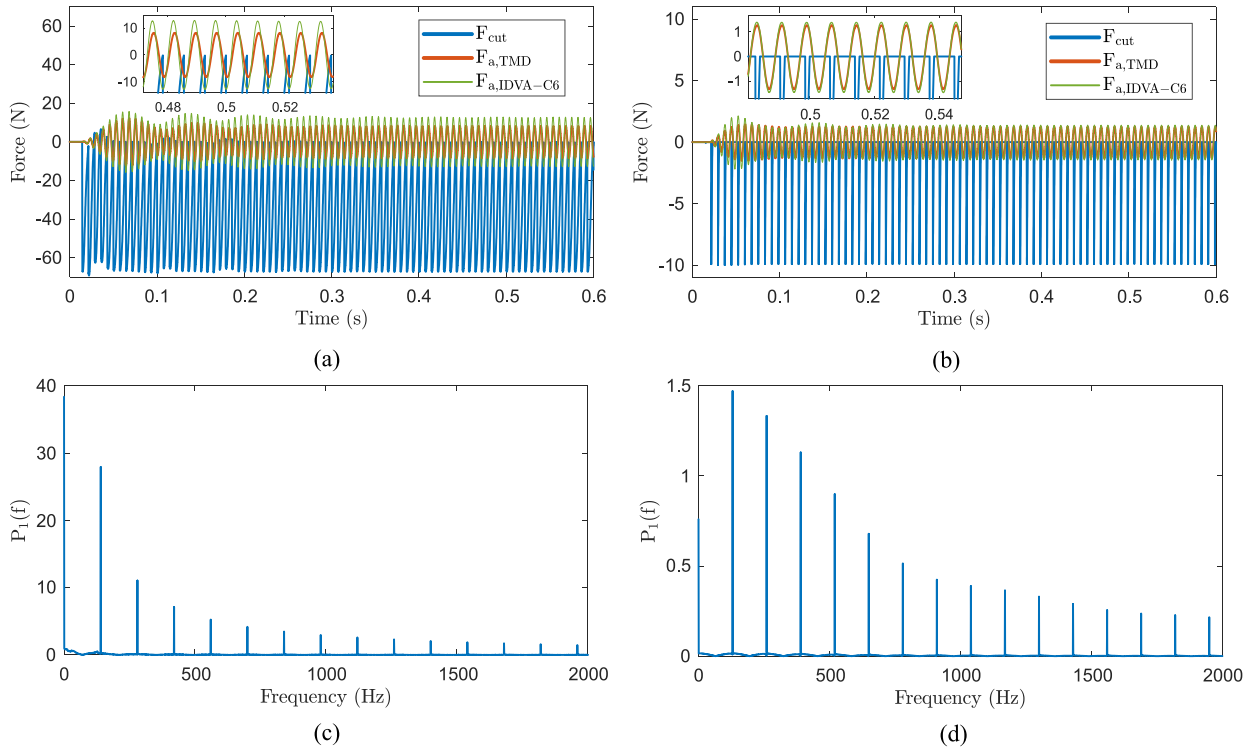|	μ	Spindle speed	Feed	Radial immersion	Axial depth of cut
Fig. 17(a)	0.0055	2100 rpm (140 Hz)	0.05 mm/tooth	50%	2 mm
Fig. 17(b)	0.05	1950 rpm (130 Hz)	0.05 mm/tooth	2%	2 mm

Fig. 17. Time domain simulations comparing two scenarios: (a) low radial immersion with $\mu = 0.0055$, $N = 2100$ rpm and 50% radial immersion, and (b) high radial immersion with $\mu = 0.05$, $N = 1950$ rpm and 2% radial immersion. The harmonics of the cutting forces obtained by the Fourier series expansion for high and low radial immersions are illustrated in frequency spectra for time domain results in (c) and (d), respectively.

References

[1] S.A. Tobias, W. Fishwick, Theory of regenerative machine tool chatter, Engineer (1958).
[2] J. Tlusty, M. Polacek, The stability of machine tools against self excited vibrations in machining, Int. Res. Prod. Eng. (1963) 465–474.
[3] R.S. Hahn, Design of lanchester damper for elimination of metal-cutting chatter, J. Eng. Ind. 73 (3) (1951) 331–335.
[4] S.A. Tobias, Machine Tool Vibration, Blackie and Sons Ltd., 1965, pp. 100–200.
[5] E.I. Rivin, H. Kang, Enhancement of dynamic stability of cantilever tooling structures, Int. J. Math. Tools Manuf. 32 (4) (1992) 539–561.
[6] Y.S. Tarng, J.Y. Kao, E.C. Lee, Chatter suppression in turning operations with a tuned vibration absorber, J. Mater Process. Technol. 105 (2000) 55–60.
[7] N.D. Sims, Vibration absorbers for chatter suppression: A new analytical tuning methodology, J. Sound Vib. 301 (2007) 592–607.

[8] M.H. Miguélez, L. Rubio, J.A. Loya, J. Fernández-Sáez, Improvement of chatter stability in boring operations with passive vibration absorbers, Int. J. Mech. Sci. 52 (10) (2010) 1376–1384.

[9] L. Rubio, J.A. Loya, M.H. Miguélez, J. Fernández-Sáez, Optimization of passive vibration absorbers to reduce chatter in boring, Mech. Syst. Signal Process. 41 (1–2) (2013) 691–704.

[10] Y. Yang, J. Muñoa, Y. Altintas, Optimization of multiple tuned mass dampers to suppress machine tool chatter, Int. J. Mach. Tools Manuf. 50 (2010) 834–842.

[11] Y. Nakano, H. Takahara, E. Kondo, Countermeasure against chatter in end milling operations using multiple dynamic absorbers, J. Sound Vib. 332 (2013) 1626–1638.

[12] Y. Yang, W. Dai, Q. Liu, Design and implementation of two-degree-of-freedom tuned mass damper in milling vibration mitigation, J. Sound Vib. 335 (2014) 78–88.

[13] Y. Yang, W. Dai, Q. Liu, Design and machining application of a two-DOF magnetic tuned mass damper, Int. J. Adv. Manuf. Technol. 89 (5–8) (2017) 1635–1643.

[14] M. Wang, T. Zan, Y. Yang, R. Fei, Design and implementation of nonlinear TMD for chatter suppression: An application in turning processes, Int. J. Mach. Tools Manuf. 50 (5) (2010) 474–479.

[15] G. Habib, G. Kerschen, G. Stépán, Chatter mitigation using the nonlinear tuned vibration absorber, Int. J. Non-Linear Mech. 91 (January) (2017) 103–112.

[16] M.C. Smith, Synthesis of mechanical networks: The inerter, IEEE Trans. Automat. Control 47 (10) (2002) 1648–1662.

[17] M.C. Smith, F.-C. Wang, Performance benefits in passive vehicle suspensions employing inerters, Veh. Syst. Dyn. 42 (4) (2004) 235–257.

[18] Y. Li, J.Z. Jiang, S.A. Neild, H. Wang, Optimal inerter-based shock–strut configurations for landing-gear touchdown performance, J. Aircr. 54 (5) (2017) 1901–1909.

[19] Y. Li, J.Z. Jiang, S. Neild, Inerter-based configurations for main-landing-gear shimmy suppression, J. Aircr. 54 (2) (2017) 684–693.

[20] K. Ikago, K. Saito, N. Inoue, Seismic control of single - degree - of - freedom structure using tuned viscous mass damper, 2012, pp. 453–474.

[21] I.F. Lazar, S.A. Neild, D.J. Wagg, Using an inerter-based device for structural vibration suppression, Earthq. Eng. Struct. Dyn. 43 (8) (2014) 1129–1147.

[22] L. Marian, A. Giaralis, Optimal design of a novel tuned mass-damper-inerter (TMDI) passive vibration control configuration for stochastically support-excited structural systems, Probab. Eng. Mech. 38 (2014) 156–164.

[23] P. Deastra, D. Wagg, N. Sims, M. Akbar, Tuned inerter dampers with linear hysteretic damping, Earthq. Eng. Struct. Dyn. 49 (12) (2020) 1216–1235.

[24] F.C. Wang, C.H. Lee, R.Q. Zheng, Benefits of the inerter in vibration suppression of a milling machine, J. Franklin Inst. B 356 (14) (2019) 7689–7703.

[25] Y. Hu, M.Z. Chen, Performance evaluation for inerter-based dynamic vibration absorbers, Int. J. Mech. Sci. 99 (2015) 297–307.

[26] H. Dogan, N.D. Sims, D.J. Wagg, Implementation of Inerter-Based Dynamic Vibration Absorber for Chatter Suppression 145 (2023) 1–10.

[27] H. Dogan, N.D. Sims, D.J. Wagg, Design, testing and analysis of a pivoted-bar inerter device used as a vibration absorber, Mech. Syst. Signal Process. 171 (February) (2022) 108893.

[28] A. Preumont, Vibration Control of Active Structures, Springer, 2018.

[29] J. Monnin, F. Kuster, K. Wegener, Optimal control for chatter mitigation in milling-part 1: Modeling and control design, Control Eng. Pract. 24 (1) (2014) 156–166.

[30] J. Monnin, F. Kuster, K. Wegener, Optimal control for chatter mitigation in milling-part 2: Experimental validation, Control Eng. Pract. 24 (1) (2014) 167–175.

[31] J.-H. Kyung, C.-W. Lee, Controller design for a magnetically suspended milling spindle based on chatter stability analysis, JSME Int. J. 46 (2) (2003) 416–422.

[32] X. Beudaert, K. Erkorkmaz, J. Munoa, Portable damping system for chatter suppression on flexible workpieces, CIRP Ann. 68 (1) (2019) 423–426.

[33] L. Sallese, G. Innocenti, N. Grossi, A. Scippa, R. Flores, M. Basso, G. Campatelli, Mitigation of chatter instabilities in milling using an active fixture with a novel control strategy, Int. J. Adv. Manuf. Technol. 89 (9–12) (2017) 2771–2787.

[34] B. Chung, S. Smith, J. Tlusty, Active damping of structural modes in high-speed machine tools, J. Sound Vib. 3 (1997) 279–295.

[35] N. Esfandi, T.-C. Tsao, Robot assisted machining of thin-walled structures, IFAC-PapersOnLine 50 (1) (2017) 14594–14599.

[36] M. Ozsoy, N. Sims, E. Ozturk, Investigation of an actively controlled robot arm for vibration suppression in milling, in: EURODYN 2020: Proceedings of the XI International Conference on Structural Dynamics, European Association for Structural Dynamics (EASD), 2020, pp. 4577–4589.

[37] M. Ozsoy, N.D. Sims, E. Ozturk, Robotically assisted active vibration control in milling: A feasibility study, Mech. Syst. Signal Process. 177 (April) (2022) 109152.

[38] J. Munoa, I. Mancisidor, N. Loix, L.G. Uriarte, R. Barcena, M. Zatarain, Chatter suppression in ram type travelling column milling machines using a biaxial inertial actuator, CIRP Ann. - Manuf. Technol. 62 (1) (2013) 407–410.

[39] I. Mancisidor, J. Munoa, R. Barcena, X. Beudaert, M. Zatarain, Coupled model for simulating active inertial actuators in milling processes, Int. J. Adv. Manuf. Technol. 77 (2015) 581–595.

[40] R. Kleinwort, M. Schweizer, M.F. Zaeh, Comparison of different control strategies for active damping of heavy duty milling operations, Proc. CIRP 46 (2016) 396–399.

[41] M.F. Zaeh, R. Kleinwort, P. Fagerer, Y. Altintas, Automatic tuning of active vibration control systems using inertial actuators, CIRP Ann. - Manuf. Technol. 66 (1) (2017) 365–368.

[42] Y. He, X. Chen, Z. Liu, Y. Chen, Active vibration control of motorized spindle based on mixed h∞Kalman filter robust state feedback control, J. Vib. Control 25 (6) (2019) 1279–1293.

[43] C.H. Yeung, Y. Altintas, K. Erkorkmaz, Virtual CNC system. Part I. System architecture, Int. J. Mach. Tools Manuf. 46 (10) (2006) 1107–1123.

[44] M. Fallah, B. Moetakef-Imani, Design, analysis, and implementation of a new adaptive chatter control system in internal turning, Int. J. Adv. Manuf. Technol. 104 (2019) 1637–1659.

[45] N.J. Van Dijk, N. Van De Wouw, E.J. Doppenberg, H.A. Oosterling, H. Nijmeijer, Robust active chatter control in the high-speed milling process, IEEE Trans. Control Syst. Technol. 20 (4) (2012) 901–917.

[46] N. van de Wouw, N. Van Dijk, A. Schiffler, H. Nijmeijer, E. Abele, Experimental validation of robust chatter control for high-speed milling processes, in: Time Delay Systems: Theory, Numerics, Applications, and Experiments, Springer, 2017, pp. 315–331.

[47] Z. Dombovari, Chatter suppression techniques in metal cutting, CIRP Ann. 65 (2) (2016) 785–808.

[48] J.N. Juang, M. Phan, Robust controller designs for second-order dynamic systems: A virtual passive approach, J. Guid. Control Dyn. 15 (5) (1992) 1192–1198.

[49] S. Huyanan, N.D. Sims, Vibration control strategies for proof-mass actuators, JVC/J. Vib. Control 13 (12) (2007) 1785–1806.

[50] Franco, M. Gil-Inchaurza, D. Barrenetxea, X. Beudaert, Virtual vibration absorber for active forced vibration reduction, CIRP Ann. (2023).

[51] Y. Altintas, E. Budak, Analytical prediction of stability lobes in milling, Ann. CIRP 44 (1) (1995) 357–362.

[52] E. Budak, Y. Altintas, Analytical prediction of chatter stability in milling — Part I : General formulation, J. Dyn. Syst. Meas. Control 120 (1998) 22–30.

[53] Y. Altintas, G. Stépán, E. Budak, T. Schmitz, Z.M. Kilic, Chatter stability of machining operations, J. Manuf. Sci. Eng.-Trans. ASME 142 (November) (2020) 1–46.

[54] K. Worden, G. Manson, On the identification of hysteretic systems. Part I: Fitness landscapes and evolutionary identification, Mech. Syst. Signal Process. 29 (2012) 201–212.

[55] M.D. McKay, R.J. Beckman, W.J. Conover, A comparison of three methods for selecting values of input variables in the analysis of output from a computer code, Technometrics 42 (1) (2000) 55–61.

[56] N.D. Sims, The self-excitation damping ratio: a chatter criterion for time-domain milling simulations, 2005.

[57] J.P. Den Hartog, Mechanical Vibrations, fourth ed., McGraw-Hill, New York, 1956.

[58] A. Bilbao-Guillerna, A. Barrios, I. Mancisidor, N. Loix, J. Munoa, Control laws for chatter suppression in milling using an inertial actuator, in: Proceedings of ISMA 2010, pp. 1–12.